Progress In Electromagnetics Research C, Vol. 125, 1–13, 2022

Design and Analysis of Compact Dual-Band Antenna System for Scalp and Skin Implantation

Moirangthem Santoshkumar Singh[1], Sourav Roy[2], Jeet Ghosh[3], Ujjal Chakraborty[4], Soumendu Ghosh[1], and Abhishek Sarkhel[1, *]

Abstract—This article proposes a compact dual-band circular-shaped implantable antenna for scalp and skin implantation applications. The proposed antenna covers the 1.395–1.432 GHz Wireless Medical Telemetry Service (WMTS) band and 2.4–2.48 GHz Industrial, Scientific, and Medical (ISM) band with a compact volume of $0.0000017\lambda_0^3$. The antenna maintains a realized peak gain of -24.5 dB and -20.6 dB, respectively, at 1.43 GHz and 2.44 GHz. Moreover, the gain pattern of the antenna is in the off-body direction which is a desirable feature for implantable scenario. It also depicts stable responses under different implantation scenarios. Moreover, the via free configuration is an advantageous feature of the proposed antenna in the context of fabrication complexity. Furthermore, a holistic design approach is considered with integrated components for device-level architecture. The resonance behavior of the proposed antenna structure is also analyzed by developing a conceptual equivalent circuit model. The evaluated specific absorption rate (SAR) complies with the regulated human safety standard. The biotelemetry link capability is also evaluated through the link margin (LM) calculation of the proposed antenna and is able to establish a communication link at a range of 4.5 m distance.

1. INTRODUCTION

The advancement in technology has considerably influenced humans' day-to-day life. In recent times, the development of biomedical devices for human health monitoring has received considerable attention [1–6]. These biomedical devices have been broadly categorized into two different categories: (1) wearable and (2) implantable/ingestible devices where the antenna has a pivotal role to play [2, 3]. Apart from wearable medical devices, researchers have taken a keen interest in the design and development of implantable medical devices (IMDs). In this regard, it is essential to note that IMDs have been developed for sensing, monitoring, stimulation, and drug delivery to improve the quality of human life [3, 4]. These devices assist in patients' diagnostic and therapeutic purposes [3]. The wireless IMDs with biotelemetry functionalities are beneficial with the integration of modern communication technology [3–5]. The wireless IMDs comprise different components, including battery, electronic circuitry, sensor, and implantable antenna.

In this context, it is worth noting that an efficient implantable antenna plays a vital role in establishing reliable communication between the IMD and external control unit. It should be noted that, unlike the traditional antenna for free-space application, designing an implantable antenna involves many challenging factors such as miniaturization, operating frequencies, specific absorption rate (SAR) for human safety, and biocompatibility with human tissue [4–6]. In this context, antenna miniaturization with desired characteristics is one of the main challenges as the space available for antenna placement in the compact implantable device is limited. In the recent past, researchers have proposed implantable

Received 12 August 2022, Accepted 23 September 2022, Scheduled 3 October 2022

* Corresponding author: Abhishek Sarkhel (abhishek.sarkhel@nitm.ac.in).

[1] National Institute of Technology Meghalaya, Shillong, India. [2] North Tripura District Polytechnic College, Dharmanagar, India. [3] Chaitanya Bharathi Institute of Technology, Hyderabad, India. [4] National Institute of Technology Silchar, Silchar, India.

antenna topologies with different miniaturization techniques, including meandered structure, spiral-shaped, shorting pin, and Planar Inverted-F antenna (PIFA) structure for various applications [4, 6, 7]. In [7], an implantable antenna has been proposed for the biomedical telemetry application at Medical Device Radiocommunications Service (MedRadio) band. In [8], an implantable antenna with 902–928 MHz Industrial, Scientific, and Medical (ISM) band operation has been proposed. An implantable antenna operating in Medical Implant Communication Service (MICS) band as a biosensor has been reported in [9]. In [10], a miniaturized implantable antenna operating at the 2.4–2.48 GHz ISM band has been proposed for biotelemetry application. However, most of these reported antennas are with linear polarization (LP) characteristics. In another aspect, researchers have also taken a keen interest in the design and development of various circular polarization (CP) implantable antennas for biomedical applications operating at the 2.4–2.48 GHz ISM band [11–14]. However, it has been reported in the recent past that the CP wave depolarizes as it traverses through the complex human tissue, which is anisotropic in nature [15]. Moreover, the implantable antennas reported in [7–14] are relatively large in size with a single band of operation which is only suitable for biotelemetry application.

Beyond single band of operation, in modern IMDs, an antenna with dual-band operation is desirable for simultaneous biomedical telemetry, wireless powering applications, etc. Many researchers have proposed implantable antennas with different topologies for dual-band operations [16–27]. Kiourti et al. proposed a circular-shaped meandered structured implantable antenna for MICS and a 2450 MHz ISM band of operation dedicated to intracranial pressure monitoring [16]. An implantable dual-band spiral dipole antenna has been proposed for the MICS band and ISM band of operations [17]. A differentially fed dual-band antenna has also been proposed for biotelemetry application in [18]. A circular-shaped implantable antenna with an operating band of 346–460 MHz and 2.37–2.63 GHz, respectively, was proposed by Mohamed et al. in [19]. A split-ring resonator (SRR) based dual-band implantable antenna for wireless power transfer and data telemetry has been proposed [21]. Despite having large impedance bandwidth, the antenna exhibits a large volume of 152.4 mm^3. PIFA configuration has been proposed for dual-band applications [22, 24]. In [22], despite the employment of the artificial neural networks (ANNs) approach, the large antenna size of 302.72 mm^3 is a point of concern. In [24], a complex shorting via configuration and an open-ended slot on the ground structure is employed to realize a circular-shaped PIFA, size miniaturization, and dual-band performance, respectively. In [25], a dual-band implantable antenna for wireless data telemetry and power transfer application has been proposed. Yamac and Basaran reported a dual-band implantable antenna based on a split ring resonator and hook-shaped slit-loaded ground plane [26]. A dual-band implantable antenna operating at 1.4 GHz Wireless Medical Telemetry Service (WMTS) band and 2.45 GHz ISM band has been proposed [27]. Most of the reported designs have a relatively large volume which compromises the compactness of the device while fabrication complexity arises due to the presence of shorting via. Thus a compact dual-band implantable antenna with a via free configuration is an utmost requirement for simultaneous wireless power transfer and biotelemetry applications.

To address the above-mentioned issues, in this article, a compact dual-band arc-slotted circular-shaped implantable antenna operating at the WMTS band and ISM band is proposed for implantable biotelemetry applications. The −10 dB impedance band of the proposed antenna covers the 1.395–1.432 GHz, WMTS band and 2.4–2.48 GHz, ISM band with a compact volume of $0.0000017\lambda_0^3$. The realized peak gain is obtained as −24.5 dB and −20.6 dB, respectively, at 1.43 GHz and 2.44 GHz resonant frequencies. The slots on the ground plane control the impedance matching as well as the shifting of both resonant frequencies. The proposed antenna has advantages over the state-of-the-art dual-band implantable antenna reported in [22–27] in terms of compactness and via free configuration with appreciable gain features. Moreover, a conceptual equivalent circuit model (ECM) of the proposed antenna structure is also developed to understand the resonance behavior of the proposed antenna configuration under an implantable scenario. Furthermore, the device level analysis is performed by integrating the proposed antenna with dummy layers for electronic circuitry and battery layer [28, 29]. The inclusion of the integrated components gives a holistic design approach. As the proposed antenna is intended for skin/scalp implantation applications that fall under the flat-type implant device category, a device-level configuration has been considered throughout the analysis. The measured response of the proposed antenna is also observed to be stable. The article has been organized as follows: initially in Section 2, the proposed antenna design mechanism and antenna analysis are illustrated. Thereafter, in

Section 3, safety regulation, communication link capacity along with in-vitro measurement results are highlighted, while the concluding discussion is presented in Section 4.

2. ANTENNA DESIGN AND ANALYSIS

2.1. Implantable Antenna Configuration

The implantable proposed antenna is designed on a 0.13 mm thick dielectric substrate ($\epsilon_r = 10.2$, $\tan\delta = 0.0035$) backed by a slotted ground plane on the other side. A 'dielectric layer 1' of similar dielectric material with the same thickness is used to cover the top radiating patch. The high dielectric material is chosen so that it assists in the miniaturization of the antenna profile by shortening the effective wavelength of the electromagnetic wave [30]. Initially, the design and simulation analysis of the antenna is performed by considering a single-layer standard size homogeneous skin phantom (HSP) model to understand the feasibility of the antenna structure. The antenna is embedded at the center with an implant depth of 3 mm from the surface of the skin. The antenna structure is excited by a 50 Ω coaxial cable. The generalized simulation model under homogeneous skin phantom is shown in Fig. 1(a). The antenna system is analyzed by implanting it inside the human phantom (head) model, which is shown in Fig. 1(b). The frequency-dependent permittivity (ϵ_r) and conductivity (σ) values of the skin tissue are considered in the simulation model [31]. A system-level flat-type implant device configuration of the proposed antenna integrated with the other dummy component is shown in Fig. 1(c). It comprises the implantable antenna, PEC-backed dielectric material as a dummy layer for electronics, power management, sensor circuitry, and PEC for a battery case. As the implant device is hostile to the human body, it is required to cover with a biocompatible material in order to prevent the undesirable short circuit and rejection by the surrounding tissues [4, 5]. Thus the components are enclosed by a 0.1 mm thick biocompatible ceramic alumina (Al_2O_3) layer. In the antenna performance analysis, different tissue layer models are considered. Figs. 1(d) and 1(e) show the single- and multi-layer tissue models for simulation analysis. The Ansys electromagnetic and Altair FEKO computational solvers are used for performing the antenna simulation analysis under different tissue models. The results of the Altair FEKO computational solver are not shown here for the sake of brevity. The resonant frequency (f_r) of a circular antenna for dominant mode TM_{110} based on the cavity model formulation illustrated in [32] is governed by Equations (1) and (2) as

$$a = \frac{F}{\left\{1 + \frac{2h}{\pi\epsilon_r F}\left[\ln\left(\frac{\pi F}{2h}\right) + 1.7726\right]\right\}^{\frac{1}{2}}} \tag{1}$$

$$F = \frac{8.791 \times 10^9}{f_r\sqrt{\epsilon_r}} \tag{2}$$

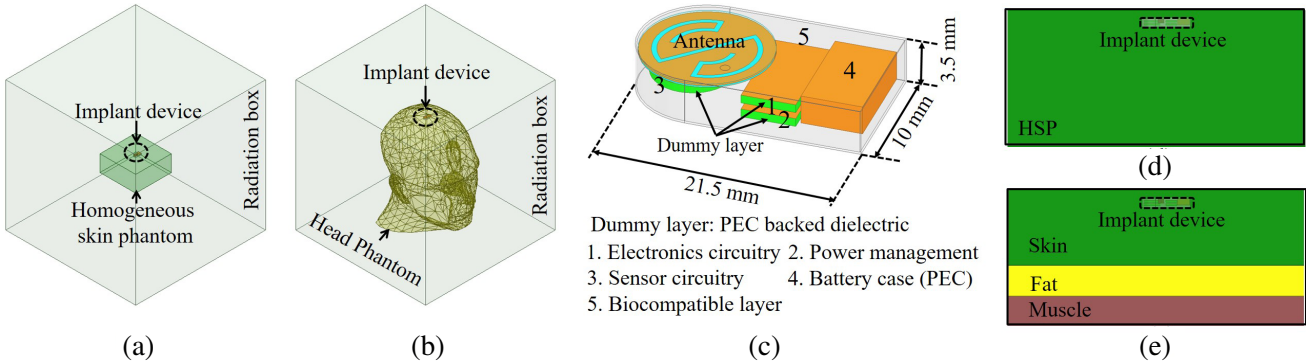

Figure 1. Simulation model of proposed antenna, (a) in homogeneous skin phantom, (b) in body phantom, (c) model of flat-type implant device, (d) single-layer tissue model, (e) multi-layer tissue model.

where a is the effective radius of the patch considering the fringing effect, and h and ϵ_r, respectively, are the thickness (in cm) and permittivity of the dielectric substrate. However, the tissue loading effect must be considered in the antenna design, which leads to a good degree of miniaturization for the implantable scenario [16]. The proposed antenna configuration and its reflection coefficient response are shown in Figs. 2(a) and 2(b), respectively. The antenna resonates at 1.43 GHz and 2.44 GHz frequency points covering the WMTS band and ISM band.

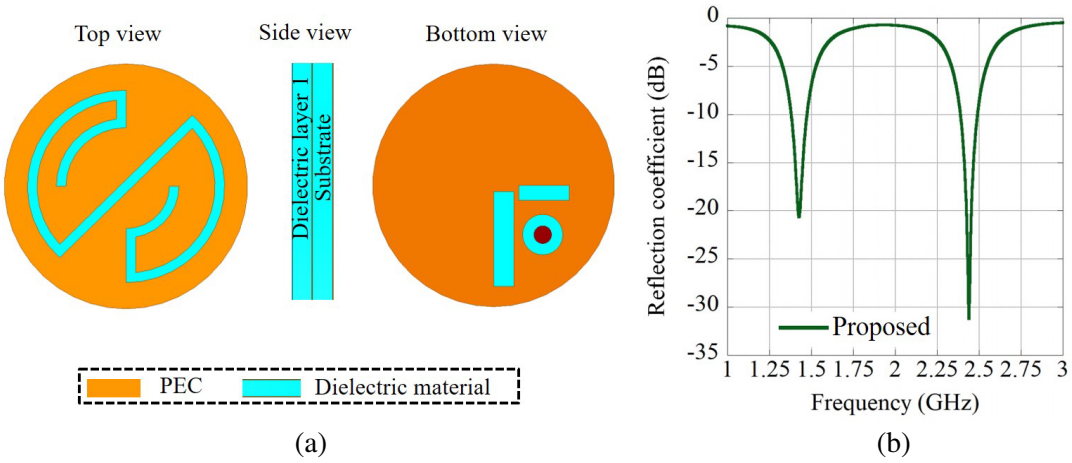

Figure 2. Proposed antenna, (a) configuration, (b) reflection coefficient response.

2.2. Design Methodology and Antenna Optimization

In the process of optimizing the proposed antenna for obtaining the desired dual-band performance for WMTS and ISM bands it passes through various developmental steps. The design and optimization of the proposed antenna involves six successive steps of structural modification on the top radiating patch and ground plane without changing the overall profile of the proposed antenna. Fig. 3 shows the developmental steps along with the geometrical configuration of the proposed antenna. The reflection coefficient response of the developmental steps with respect to frequency is shown in Fig. 4. The antenna performance is significantly improved through each stage of modification. The design starts with a circular patch antenna as step 1, where the structure shows a poor impedance matching at 4.43 GHz frequency as shown in Fig. 4(a). However, it requires miniaturization with good impedance

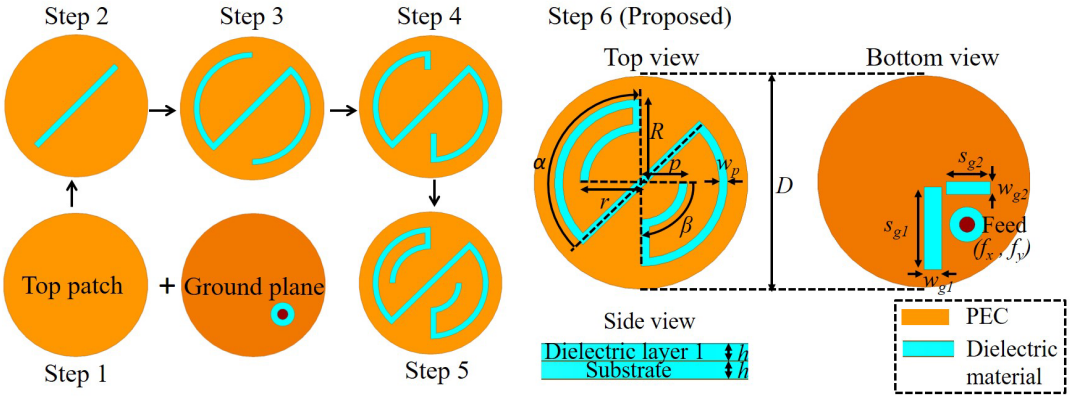

Figure 3. Developmental steps and geometrical configuration of the proposed antenna [$D = 9.6$, $R = 3.772$, $r = 2.755$, $p = 2.09$, $w_p = 0.4$, $h = 0.13$, $s_{g1} = 3.75$, $s_{g2} = 2$, $w_{g1} = 0.8$, $w_{g2} = 0.6$, $(f_x, f_y) = (1.95, 1.95)$, (unit: mm, coordinate origin: center of the patch), $\alpha = 135°$, $\beta = 90°$].

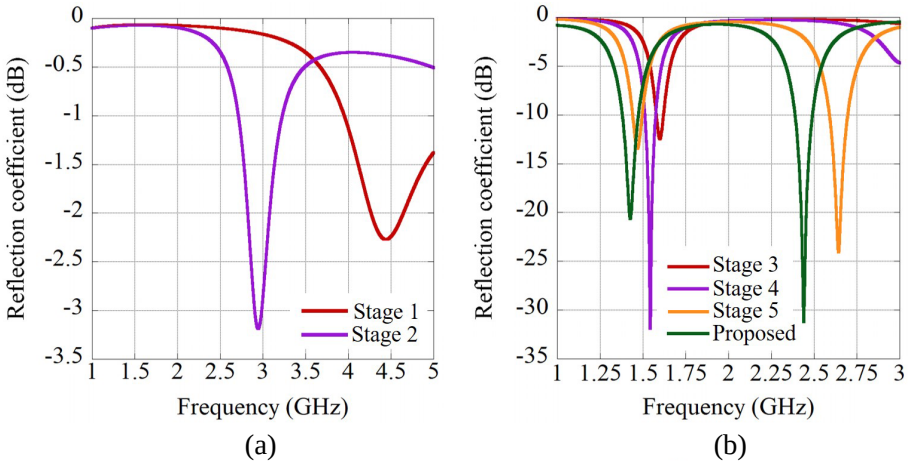

Figure 4. Reflection coefficient of the antenna developmental steps, (a) steps 1–2, (b) steps 3–6.

matching performance towards the desired frequencies. In step 2, a diagonal slot is loaded at the center of the radiating patch which drives the current path towards the edge of the structure near the end of the diagonal slot. As a result of this modification, the frequency is shifted towards 2.95 GHz which suggests miniaturization, but the matching level is still poor. Therefore, it is required to optimize further as the present 2.95 GHz band does not fall under the desired band of interest. Therefore, a pair of symmetric arc-shaped slots are introduced in the clockwise direction from both ends of the diagonal slot in step 3. The lengthened current path with this modification results in the miniaturization of the resonance with improvement in the impedance matching to 1.6 GHz. However, the antenna sticks to a single band of operation. In step 4, the current path is further lengthened by extending the length of the arc-shaped slot vertically at both ends, which results in further miniaturization of the resonance to 1.54 GHz with improved impedance matching. Moreover, a weak resonance is observed in the vicinity of 3 GHz with a matching level of −5 dB. However, this band requires further tuning for the desired WMTS band of operation. Thus, in step 5 the symmetric arc-shaped slot is elongated by a pair of asymmetric arc-shaped slots in a counter-clockwise direction from both ends. The lengthened current path with this modification not only results in the miniaturization of both resonances but also improves the impedance matching at higher frequency regions. However, the reflection coefficient response does not cover the desired band of interest. Therefore, in the final step 6, two slots are incorporated on the ground plane of the previous structure, and the proposed antenna structure is obtained, as shown in Fig. 3. It is observed from Fig. 4 that with the incorporation of these slots on the ground plane, the resonant frequencies are shifted to the two desired frequency bands with improved impedance matching performance. The optimized proposed antenna is operating in the frequency range of 1.390–1.470 GHz and 2.39–2.49 GHz that covers the WMTS and ISM bands, respectively. The −10 dB impedance bandwidth at lower and higher resonant frequencies region is obtained as 80 MHz and 100 MHz, respectively with a compact volume of $0.0000017\lambda_0^3$. The optimized dimensional values are listed in the figure caption of Fig. 3.

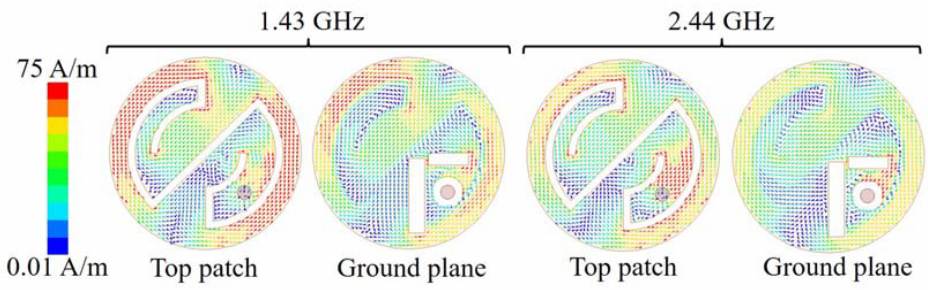

Figure 5. Surface current distribution of the proposed antenna.

The working principle of the proposed antenna can be understood from the surface current distributions as shown in Fig. 5. It is observed that the peripheral area near the symmetric arc-shaped slot in the top patch is highly excited at 1.43 GHz, which contributes to the lower resonance frequency, whereas the area near the feed between the two arc-shaped slots is highly excited which is primarily responsible for 2.44 GHz. The simulated peak gain at 1.43 GHz and 2.44 GHz is obtained as −24.5 dB and −20.6 dB, respectively, which is shown in Figs. 6(a) and 6(b). The 3D radiation pattern shown in Fig. 7 indicates that the proposed antenna radiates in the off-body direction, which is desirable for implantable scenario.

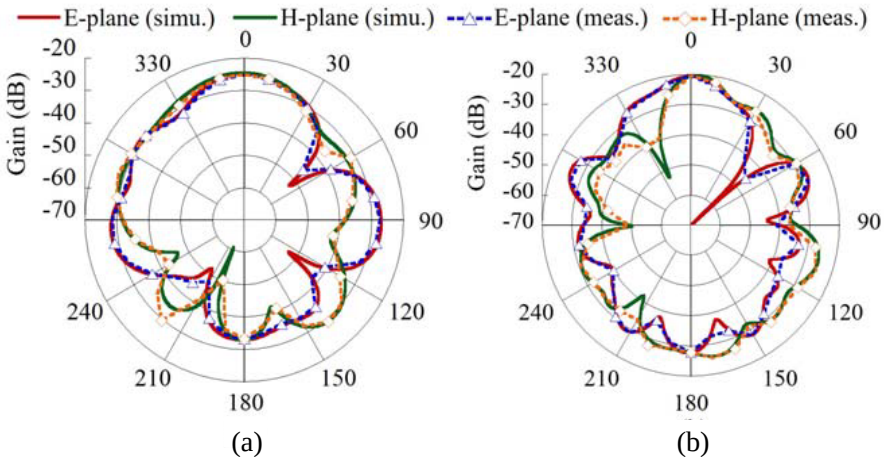

Figure 6. Far-field pattern of the proposed antenna, (a) 1.43 GHz, (b) 2.44 GHz.

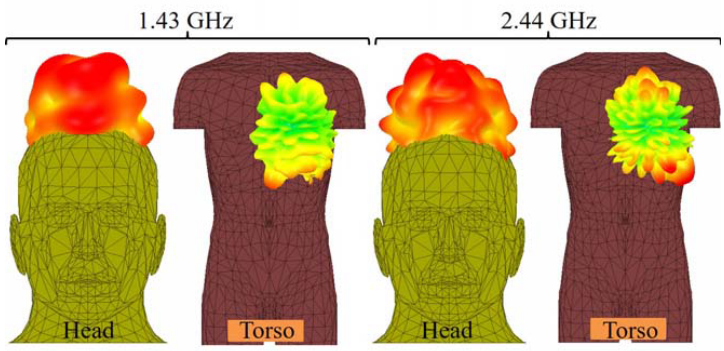

Figure 7. 3D pattern of the proposed antenna for different implant position.

2.3. Sensitivity of the Antenna Response with Parametric Variations

2.3.1. Variation of α and β

In order to obtain a better performance antenna, sensitive antenna parameters which can affect the reflection coefficient of the proposed antenna is analyzed. The analysis is performed by keeping the other parameters constant except the relevant key parameter without modifying the antenna profile. The response of the proposed antenna is analyzed with the variation of the parameters α and β, which defines the length of the arc-shaped slot at the radiating patch. The length of the arc-shaped slot influences both the lower and higher resonant frequencies of the antenna. When the length of the arc-shaped slot increases, the associated current path is lengthened which results in the shifting of both resonant frequencies on the lower side which is shown in Fig. 8(a). The good performance of lower and higher resonant frequency bands is observed when $\alpha = 135°$ and $\beta = 90°$ covering the desired WMTS

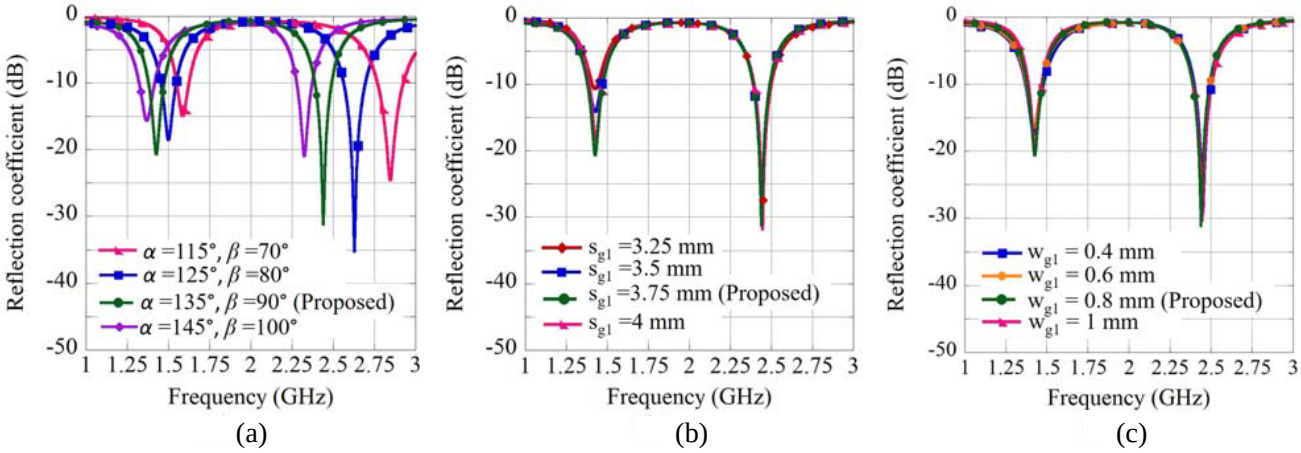

Figure 8. Response of the proposed antenna with the variation of (a) α, β, (b) s_{g1}, (c) w_{g1}.

and ISM bands. These values are considered and optimized for the proposed antenna. However, the antenna performance is not only dependent on the α and β parameters but also dependent on the other parameters which will be discussed further.

2.3.2. Variation of s_{g1}, w_{g1}, s_{g2} and w_{g2}

In order to understand the dependency of antenna performance on parameters s_{g1}, w_{g1}, s_{g2}, and w_{g2}, further, the analysis is performed. It is clear from Fig. 8(b) that the variation of parameter s_{g1} does not shift the lower and higher resonant frequencies, but controls the impedance matching level at the lower resonant frequency. On the other hand, there is no significant variation in both the resonant frequency regions with the variation of parameter w_{g1}, which is shown in Fig. 8(c). However, the variation in parameter s_{g2} influences the impedance matching at both the lower and higher resonant frequencies with slight shifting of the higher resonant frequency, which can be seen in Fig. 9(a). Fig. 9(b) shows the antenna response with the variation of parameter w_{g2}. It can be seen from the figure that the impedance matching level at lower resonant frequency varies with parameter w_{g2}, but both the lower and higher resonant frequencies do not shift with this variation. It suggests that the slots on the ground plane influence the tuning of resonant frequencies as well as control the impedance matching in both the resonant frequencies. The variations in the reflection coefficient suggest the variation in corresponding input impedance. The same has been optimized to cover the desired band.

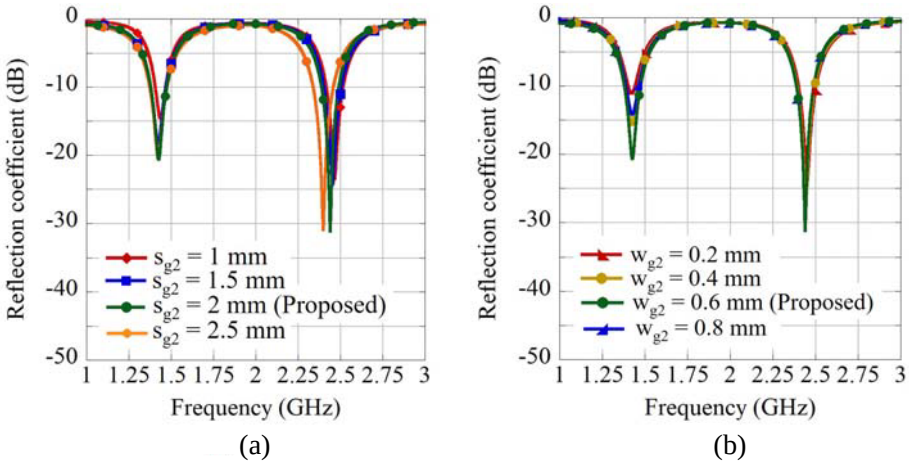

Figure 9. Response of the proposed antenna with the variation of (a) s_{g2}, (b) w_{g2}.

2.3.3. Multi-Layered Tissue Model

To understand the sensitivity of the proposed antenna in a complex tissue model, a simulation analysis is performed in the three-layered tissue model comprising skin, fat, and muscle. The thickness of the individual tissue layer is taken from the three-layered model reported in [14], where the overall thickness is close to that of HSP. The three-layered tissue model for simulation is shown in Fig. 10(a). The antenna response is analyzed by embedding the antenna in the different tissue layers, and their corresponding reflection coefficient response is shown in Fig. 10(b). The muscle tissue's effective permittivity is slightly higher than the skin tissue; thus, the resonant frequency is shifted towards the lower frequency region. Moreover, the shifting of resonance still covers the desired band. Likewise, the effective permittivity of the fat tissue is very small as compared to the skin/muscle tissue, and thus the resonant frequency is significantly shifted towards the higher frequency region.

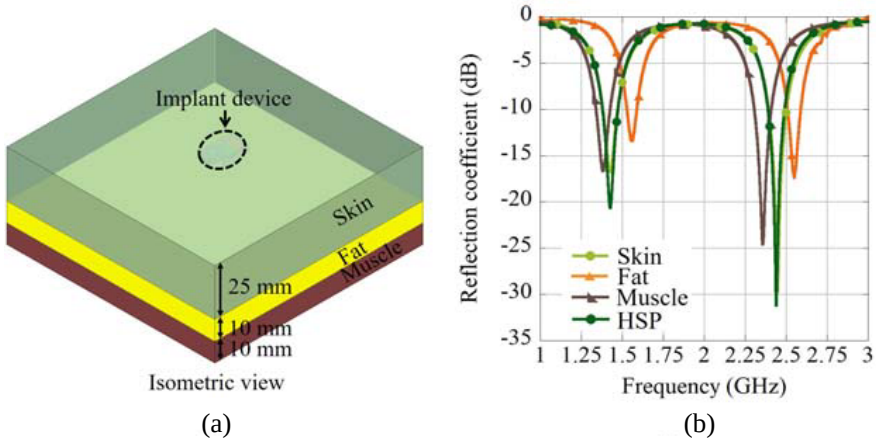

Figure 10. Simulation model of proposed antenna (a) three-layered tissue model, (b) reflection coefficient response.

2.4. Equivalent Circuit Model

A conceptual equivalent circuit model (ECM) is developed to understand the resonance behavior of the proposed antenna. Fig. 11(a) shows the lumped component ECM of the proposed antenna. Each of

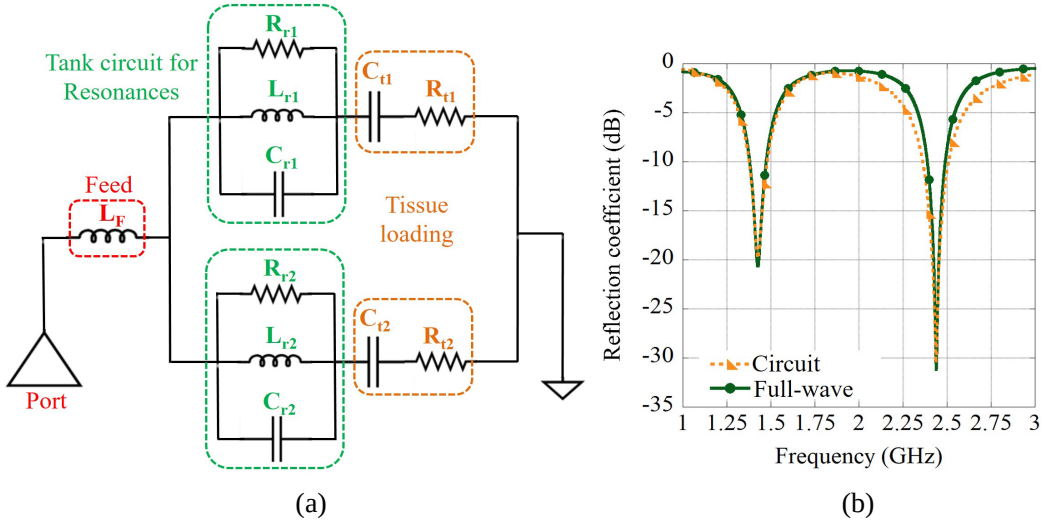

Figure 11. Proposed antenna (a) equivalent circuit model, (b) reflection coefficient response.

the resonant frequency of the proposed antenna can be modeled as a parallelly connected RLC (tank) circuit [29]. In the ECM, L_F is the inductance of the antenna due to the feeding network, whereas each parallel RLC network represents the individual resonance. R_{r1} and R_{r2} represent the resistance of the corresponding individual resonance. The presence of human tissue introduces a loading effect modeled as capacitive loading which is represented by C_{t1} and C_{t2} in the ECM, whereas the loss introduced is modeled as a resistive effect which is represented by R_{t1} and R_{t2} in the ECM. The ADS tool is used to extract the lumped component parameters, and their values are listed as $L_F = 1.2\,\text{nH}$, $R_{r1} = 90\,\Omega$, $L_{r1} = 2.7\,\text{nH}$, $C_{r1} = 1.1\,\text{pF}$, $R_{r2} = 90\,\Omega$, $L_{r2} = 1\,\text{nH}$, $C_{r2} = 5.5\,\text{pF}$, $C_{t1} = 19.5\,\text{pF}$, $R_{t1} = 1\,\Omega$, $C_{t2} = 2.7\,\text{pF}$, $R_{t2} = 1\,\Omega$. Fig. 11(b) shows the response of the equivalent circuit model analysis of the proposed antenna. It is observed from the figure that the equivalent circuit analysis shows a good degree of consistency with the electromagnetic full-wave analysis.

3. SAFETY REGULATION, COMMUNICATION LINK AND MEASUREMENT RESULTS

3.1. SAR Evaluation

To ensure the patient's safety, the SAR needs to maintain the regulated standard. The IEEE standard regulation restricts a maximum SAR of 1.6 W/kg for 1 g and 2 W/kg for 10 g average tissues [33, 34]. The SAR distributions analysis is performed for the target frequency using the human head and torso model present in the Ansys electromagnetic solver. An implant depth of 3 mm has been considered as the target application for the skin/scalp implantation scenario. Figs. 12(a) and 12(b) show the simulated

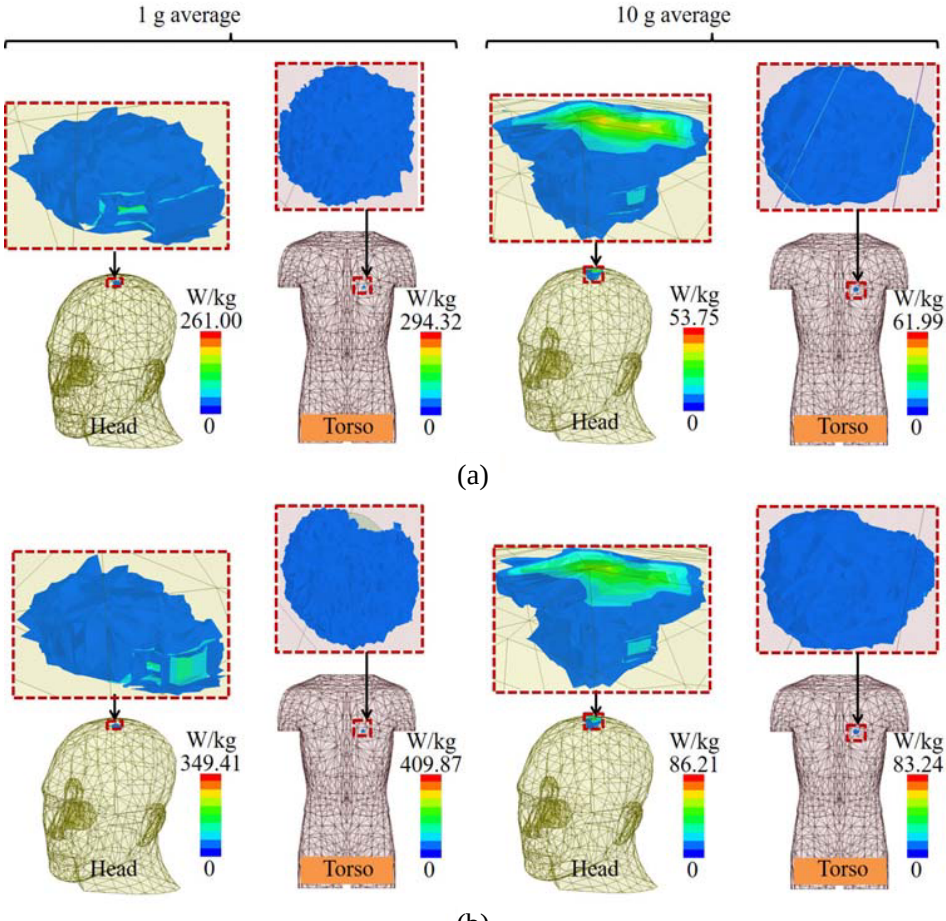

Figure 12. Simulated SAR values at (a) 1.43 GHz, (b) 2.44 GHz for different implant positions.

SAR at 1.43 GHz and 2.44 GHz for the human head and torso model for 1 g and 10 g averaged tissue, respectively. The simulated maximum SAR values and acceptable net input power at 1.43 GHz and 2.44 GHz for 1 g and 10 g average tissue are tabulated in Table 1. It is evaluated that the maximum acceptable input power is 4.57 mW and 21.19 mW for 1 g and 10 g average tissue, respectively, for the scalp implantation scenario, whereas 3.9 mW and 24.02 mW for 1 g and 10 g average tissue, respectively, for the skin implantation scenario.

Table 1. Simulated SAR and maximum acceptable input power (input power = 1 W).

Frequency (GHz)	Phantom model	SAR (W/kg)		max. input power (mW)	
		1 g average	10 g average	1 g average	10 g average
1.43	Head	261	53.75	6.13	37.2
	Torso	294.32	61.99	5.43	32.26
2.44	Head	349.41	86.21	4.57	21.19
	Torso	409.87	83.24	3.9	24.02

3.2. Link Margin Evaluation for Biotelemetry Link

The communication ability range of the proposed implantable antenna with the external receiver antenna at a distance of 'd' is investigated by evaluating the link margin (LM). The LM, according to Friis Transmission Formula, as mentioned in [11, 35], is calculated as:

$$\text{LM} = \text{Link}\frac{C}{N_0} - \text{Required}\frac{C}{N_0} \tag{3}$$

$$= P_t + G_t - L_f + G_r - N_0 - \frac{E_b}{N_0} - 10\log_{10} B_r + G_c - G_d \tag{4}$$

where

$$L_f = 20\log_{10}\frac{4\pi d}{\lambda} \tag{5}$$

The input power, P_t, is restricted to 25 µW under European Research Council regulation [28]. The receiver gain G_r is considered as 2.15 dBi for a standard dipole antenna [28]. L_f is the path loss, N_0 the noise power, and B_r the bit rate. Other than the transmitter gain G_t and resonance frequency, the parameters for LM calculation are considered from [35]. For reliable communication, the 20 dB LM is

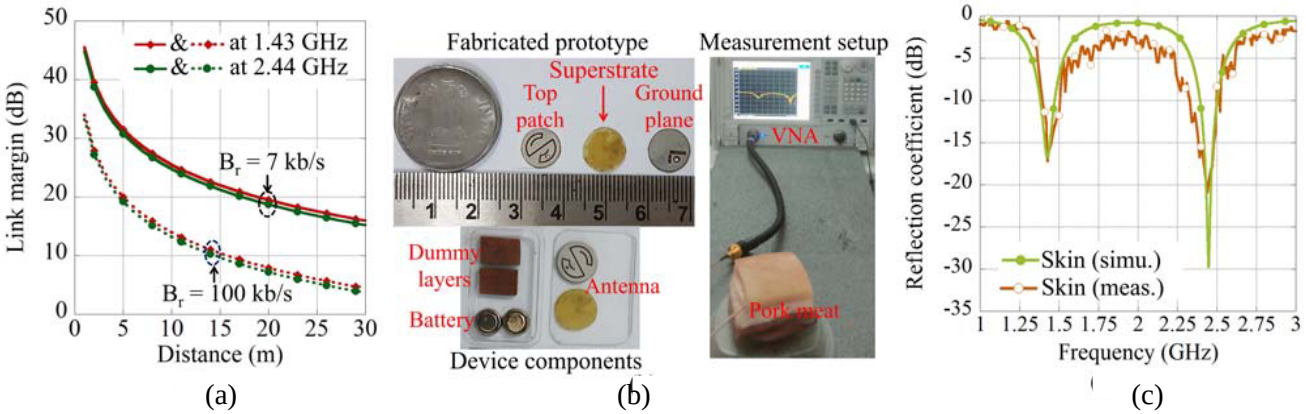

Figure 13. Proposed antenna. (a) Link margin. (b) Fabricated prototype along with device components and the antenna under measurement environment. (c) Reflection coefficient response at different tissue layers [simu.: simulated, meas.: measured].

considered. It is observed from Fig. 13(a) that a communication range of up to 17 m is achieved with a data transmission rate of 7 kb/s (for pressure data) at 1.43 GHz. Moreover, increasing the bit rate to 100 kb/s for higher data transmission can cover at least a distance of 4.5 m.

3.3. Antenna Measurement and Discussion

To validate the proposed antenna performance for a realistic environment, in-vitro measurement is performed by placing the fabricated antenna inside a pork meat chunk using the PNA Network Analyzer N5221A. The fabricated prototype and measurement setup of the proposed antenna are shown in Fig. 13(b). The slight differences in the simulation and measurement responses which can be seen in Fig. 13(c) are due to the fabrication and measurement tolerance. The measured peak gains at 1.43 GHz and 2.44 GHz are −25 dB and −20.5 dB, respectively, as shown in Figs. 6(a) and 6(b), which is in good agreement with the simulated values.

3.4. Comparison of Antenna Performance

The comparative status of the proposed antenna with respect to the present state-of-the-art dual-band implantable antenna in the literature is outlined in Table 2. It is clear that the proposed antenna exhibits a compact size with relatively higher gain than that reported in [22–27].

Table 2. Proposed implantable antenna with respect to the state-of-the-art dual-band antenna.

Ref.	Physical volume	f_r, Application band	BW	Gain (dBi)	SAR (W/kg)		ECM analysis?	Shorting Pin/Via?
					1 g avg.	10 g avg.		
[22]	302.72 mm^3	402 MHz, MedRadio 915 MHz, ISM	7.44% 5.25%	−31.6 −21	— —	— —	No	Yes
[23]	1459.5 mm^3	403 MHz, MICS 2.45 GHz, ISM	18.4% 40.8%	−33 −16	603.62 330.41	65.72 39.95	No	Yes
[24]	120.432 mm^3	402 MHz, MedRadio 2.45 GHz, ISM	8.4% 27.8%	−35.9 −21.3	666 676	— —	No	Yes
[25]	284.48 mm^3	402 MHz, MedRadio 915 MHz, ISM	8.4% 5.7%	−35.9 −24.3	293.7 —	74.1 —	No	Yes
[26]	153.35 mm^3	402 MHz, MedRadio, ISM 2.4 GHz, ISM	53% 9%	−38.08 −22.03	307 312	—	No	Yes
[27]	103.7 mm^3	1.4 GHz, WMTS 2.45 GHz, ISM	10.38% 21.3%	−32 −31.6	—	—	No	Yes
Proposed antenna	18.8 mm^3	1.43 GHz, WMTS 2.44 GHz, ISM	6.31% 3.27%	−24.5 −20.6	261(H) 294.32(T) 349.41(H) 409.87(T)	53.75(H) 61.99(T) 86.21(H) 83.24(T)	Yes	No

f_r: resonant frequency, BW: Impedance bandwidth, (H): in human head model, (T): in human torso model

4. CONCLUSION

A compact dual-band arc-slotted circular-shaped implantable antenna is proposed for implantable applications. The proposed antenna performance covers the 1395–1432 MHz WMTS band and 2.4–2.48 GHz ISM band. The antenna attained a measured peak gain of −25 dB and −20.5 dB at 1.43 GHz and 2.44 GHz frequency bands, respectively. The via free configuration is also an advantageous feature of this work in the context of fabrication complexity with a noticeable reduction of physical size. The flat-type device configuration of the proposed antenna is analyzed to give a holistic design approach for a realistic scenario. The simulated SAR also complies with the regulated human safety standard. In addition, the LM of the proposed antenna is evaluated, and it is able to communicate up to 17 m

distance with a data transmission rate of 7 kb/s and 4.5 m distance with a data transmission rate of 100 kb/s, respectively. A good degree of consistency is observed between the measured response of the proposed antenna and the simulated response.

ACKNOWLEDGMENT

The authors would like to acknowledge Center of Excellence on Wireless Communication of National Institute of Technology Meghalaya for assisting in the measurement process of the antenna.

REFERENCES

1. Khattak, R. Y., Q. Ahmed, S. Shoaib, and M. Hafeez, "Array antenna for wireless access points and futuristic healthcare devices," *Electronics*, Vol. 11, No. 8, 1226, 2022.
2. Kumar, P., T. Ali, and A. Sharma, "Flexible substrate based printed wearable antennas for wireless body area networks medical applications," *Radioelectronics and Communications Systems*, Vol. 64, No. 7, 337–350, 2021.
3. Kiourti, A., K. A. Psathas, and K. S. Nikita, "Implantable and ingestible medical devices with wireless telemetry functionalities: A review of current status and challenges," *Bioelectromagnetics*, Vol. 35, No. 1, 1–15, 2014.
4. Kiourti, A. and K. S. Nikita, "A review of implantable patch antennas for biomedical telemetry: Challenges and solutions [wireless corner]," *IEEE Antennas and Propagation Magazine*, Vol. 54, No. 3, 210–228, 2012.
5. Kiourti, A. and K. S. Nikita, "A review of in-body biotelemetry devices: Implantables, ingestibles, and injectables," *IEEE Transaction on Biomedical Engineering*, Vol. 64, No. 7, 1422–1430, 2017.
6. Malik, N. A., P. Sant, T. Ajmal, and M. Ur-Rehman, "Implantable antennas for bio-medical applications," *IEEE Journal of Electromagnetics, RF and Microwaves in Medicine and Biology*, Vol. 5, No. 1, 84–96, 2021.
7. Li, H., Y.-X. Guo, C. Liu, S. Xiao, and L. Li, "A miniature-implantable antenna for MedRadio-band biomedical telemetry," *IEEE Antennas and Wireless Propagation Letters*, Vol. 14, 1176–1179, 2015.
8. Luan, Z., L. Liu, W.-H. Zong, Z. Jin, and S. Li, "Design of an implantable antenna operating at ISM band using magneto-dielectric material," *Progress In Electromagnetics Research Letters*, Vol. 82, 65–72, 2019.
9. Khadase, R. B., A. Nandgaonkar, B. Iyer, and A. E. Wagh, "Multilayered implantable antenna biosensor for continuous glucose monitoring: Design and analysis," *Progress In Electromagnetics Research C*, Vol. 114, 173–184, 2021.
10. Singh, M. S., J. Ghosh, S. Ghosh, and A. Sarkhel, "Miniaturized dual-antenna system for implantable biotelemetry application," *IEEE Antennas and Wireless Propagation Letters*, Vol. 20, No. 8, 1394–1398, 2021.
11. Liu, X. Y., Z. T. Wu, Y. Fan, and E. M. Tentzeris, "A miniaturized CSRR loaded wide-beamwidth circularly polarized implantable antenna for subcutaneous real-time glucose monitoring," *IEEE Antennas and Wireless Propagation Letters*, Vol. 16, 577–580, 2017.
12. Yang, Z.-J., S.-Q. Xiao, L. Zhu, B.-Z. Wang, and H.-L. Tu, "A circularly polarized implantable antenna for 2.4-GHz ISM band biomedical applications," *IEEE Antennas and Wireless Propagation Letters*, Vol. 16, 2554–2557, 2017.
13. Li, R., Y.-X. Guo, B. Zhang, and G. Du, "A miniaturized circularly polarized implantable annular-ring antenna," *IEEE Antennas and Wireless Propagation Letters*, Vol. 16, 2566–2569, 2017.
14. Saha, P., D. Mitra, and S. K. Parui, "A circularly polarised implantable monopole antenna for biomedical applications," *Progress In Electromagnetics Research C*, Vol. 85, 167–175, 2018.
15. Bao, Z., "Comparative study of dual-polarized and circularly-polarized antennas at 2.45 GHz for ingestible capsules," *IEEE Transactions on Antennas and Propagation*, Vol. 67, No. 3, 1488–1500, 2019.

16. Kiourti, A., K. A. Psathas, J. R. Costa, C. A. Fernandes, and K. Nikita, "Dual-band implantable antennas for medical telemetry: A fast design methodology and validation for intra-cranial pressure monitoring," *Progress In Electromagnetics Research*, Vol. 141, 161–183, 2013.
17. Xu, L.-J., Y.-X. Guo, and W. Wu, " Miniaturized dual-band antenna for implantable wireless communications," *IEEE Antennas and Wireless Propagation Letters*, Vol. 13, 1160–1163, 2014.
18. Liu, Y., Y. Chen, H. Lin, and F. H. Juwono, "A novel differentially fed compact dual-band implantable antenna for biotelemetry applications," *IEEE Antennas and Wireless Propagation Letters*, Vol. 15, 1791–1794, 2016.
19. Mohamed, A. E., M. S. Sharawi, and A. Muqaibel, "Implanted dual-band circular antenna for biomedical applications," *Microw. Opt. Technol. Lett.*, Vol. 60, 1125–1132, 2018.
20. Hashemi, S. and M. J. Rashed, "Miniaturization of dual band implantable antennas," *Microw. Opt. Technol. Lett.*, Vol. 59, No. 1, 36–40, 2017.
21. Zhang, H., L. Li, C. Liu, Y.-X. Guo, and S. Wu, "Miniaturized implantable antenna integrated with split resonate rings for wireless power transfer and data telemetry," *Microw. Opt. Technol. Lett.*, Vol. 59, No. 3, 710–714, 2017.
22. Djellid, A., L. Pichon, S. Koulouridis, and F. Bouttout, "Miniaturization of a PIFA antenna for biomedical applications using artificial neural networks," *Progress In Electromagnetics Research M*, Vol. 70, 1–10, 2018.
23. Basir, A., A. Bouazizi, M. Zada, A. Iqbal, S. Ullah, and U. Naeem, "A dual-band implantable antenna with wide-band characteristics at MICS and ISM bands," *Microw. Opt. Technol. Lett.*, Vol. 60, No. 12, 2944–2949, 2018.
24. Luo, L., B. Hu, J. Wu, T. Yan, and L.-J. Xu, "Compact dual-band antenna with slotted ground for implantable applications," *Microw. Opt. Technol. Lett.*, Vol. 61, No. 5, 1314–1319, 2019.
25. Bakogianni, S. and S. Koulouridis, "A dual-band implantable rectenna for wireless data and power support at sub-GHz region," *IEEE Transactions on Antennas and Propagation*, Vol. 67, No. 11, 6800–6810, 2019.
26. Yamac, Y. E. and S. C. Basaran, "An SRR based miniature implantable antenna with a slit loaded ground at MedRadio and ISM bands for biotelemetry applications," *Int. J. RF Microw. Comput. Aided Eng.*, Vol. 30, No. 11, e22406, 2020.
27. Xu, L.-J., Z.-J. Chu, L. Zhu, J.-P. Xu, and Z. Duan, "Design and analysis of dual-band implantable antennas based on effective relative permittivity calculation," *IEEE Transactions on Antennas and Propagation*, Vol. 69, No. 5, 2463–2472, 2021.
28. Shah, S. A. A. and H. Yoo, "Scalp-implantable antenna systems for intracranial pressure monitoring," *IEEE Transactions on Antennas and Propagation*, Vol. 66, No. 4, 2170–2173, 2018.
29. Basir, A. and H. Yoo, "A stable impedance-matched ultrawideband antenna system mitigating detuning effects for multiple biotelemetric applications," *IEEE Transactions on Antennas and Propagation*, Vol. 67, No. 5, 3416–3421, 2019.
30. Cui, W., Z. Li, C. Fan, M. Wang, H. Zheng, and E. Li, "Design of circularly polarized implantable antenna for wireless intracranial pressure monitoring system," *Int. J. RF Microw. Comput. Aided Eng.*, Vol. 32, No. 4, e23053, 2022.
31. Gabriel, S., R. W. Lau, and C. Gabriel, "The dielectric properties of biological tissues: II. Measurements in the frequency range 10 Hz to 20 GHz," *Physics in Medicine and Biology*, Vol. 41, 2251–2269, 1996.
32. Balanis, C. A., *Antenna Theory: Analysis and Design*, 3rd Edition, John Wiley & sons, 2005.
33. IEEE Standard for Safety Levels with Respect to Human Exposure to Radio Frequency Electromagnetic Fields, 3 kHz to 300 GHz, IEEE Std C95.1-1999, 1999.
34. IEEE Standard for Safety Levels with Respect to Human Exposure to Radio Frequency Electromagnetic Fields, 3 kHz to 300 GHz, (Revision of IEEE Std C95.1-1991), 2006.
35. Yin, B., M. Ye, J. Cong, and Y. Xu, "A miniaturized dual-band circularly polarized implantable antenna by half-cutting," *Progress In Electromagnetics Research M*, Vol. 108, 139–149, 2022.